Available online at www.sciencedirect.com
ScienceDirect
Ceramics International 38 (2012) 401–409
CERAMICS INTERNATIONAL
www.elsevier.com/locate/ceramint

Mechanical characterization at nanometric scale for heterogeneous graphite–salt phase change materials with a statistical approach

V. Canseco [a], J.J. Roa [b,*], E. Rayón [c], A.I. Fernández [d], E. Palomo [a]

[a] Institut de Mecanique et d'Ingenierie de Bordeaux I2M, Departement Trefle, UMR-CNRS 8508, Site ENSAM-Esplanade des Arts et Metiérs, 33405 Talence, France
[b] Institut Pprime. Departement Physique et Mecanique des Materiaux, Branche Physique des Materiaux. CNRS-Université de Poitiers-ENSMA, UPR 3346, Boulevard Marie et Pierre Curie, 86962 Futuroscope Chasseneuil Cedex, France
[c] Instituto de Tecnologia de Materiales, Universidad Politecnica de Valencia, Cami de Vera s/n, E-46022 Valencia, Spain
[d] Centre Diopma Universidad de Barcelona, Facultad de Quimica, Departamento de Ciencia de los Materiales e Ing. Metalurgica, C/Martí i Franquès, 1, 08028 Barcelona, Spain

Received 20 June 2011; received in revised form 8 July 2011; accepted 8 July 2011
Available online 19th July 2011

Abstract

A statistical indentation analysis of a series of phase change graphite–salt composite materials for latent heat thermal energy storage applications was investigated using instrumented indentation technique with the aim of isolate the mechanical influence of each phase. This method employs the instrumented indentation technique to extract the in situ hardness and Young's modulus properties of individual components without the need to observe the residual imprints for heterogeneous materials. This approach relies on a large array of imprints (around 1000 indentations performed at 200 nm of indentation depth) and the statistical analysis of the resulting data. A statistical study by a Cumulative Distribution Function fit and Gaussian simulated distributions showed that the mechanical properties for each compound can be isolated when the indentation depth is much lower than the size of the secondary phases.

Keywords: Instrumented indentation technique; Statistical method; Heterogeneous materials; Hardness; Young's modulus; Phase change materials

1. Introduction

Thermal energy storage has experienced a fast development in recent years since it represents a key technology for present and future applications. Today, producing energy from the sun is not the only priority, indeed storing it has also become a major objective. The core of energy storage technologies based upon latent heat is the phase change material (PCM) [1,2]. Choosing the right type of PCM among the wide range of available options depends firstly on the desired application. For instance, some materials are better suited for thermal storage at low temperatures like paraffin waxes which are widely used for improving energy efficiency in buildings [3,4]. Salts are also a common PCM with interesting properties such as high energy densities and a wide range of working temperatures which make them good candidates for several applications, including energy storage at high temperatures [5,6]. In general, the literature [2] points that selecting the appropriate PCM for a given application must rely on physical, technical and economical requirements.

In our case, a composite PCM made of salt and graphite foam has already been chosen as a candidate for energy storage through latent heat. The context in which this composite will be working is electricity generation in solar power plants equipped with an energy storage module [7]. As mentioned earlier, the selected material should cover several requirements; here we are particularly interested in measuring the mechanical properties of the PCM at the micro scale making this task the principal objective of the present work. The obtained data will be used to determine whether or not the structure of the composite will stand against the different constraints that appear during working conditions, such as the pressure that develops inside the PCM when the change phase takes place or the pressure coming from the outside related to the storage module selected configuration.

* Corresponding author.
E-mail address: jjrr_cons@hotmail.com (J.J. Roa).

0272-8842/$36.00
doi:10.1016/j.ceramint.2011.07.021

The micro scale characterization was performed with the nanoindentation technique, thus a brief description of this technique as well as its basic concepts is presented.

Nanoindentation or instrumented indentation technique (IIT) is a powerful technique that provides useful information about the mechanical properties of materials at the micro scale. This tool has been widely employed in the past two decades [8,9] for isolating the mechanical response to either layered materials [10,11] or homogeneous samples [12]. During the last years some authors [13] have extended the applicability of this technique to heterogeneous materials [14]. Such properties are obtained by evaluating the response of the sample to an applied load as a function of its magnitude or its indentation depth. This concept is not new since hardness tests [15] are based on the same principle, nevertheless the innovation accomplished by nanoindentation relies on two main achievements: the developing of new machines capable of recording small loads and displacements with high accuracy and precision and the implementation of analytical models for interpreting and analyzing the load–displacement (or P–h) data. By combining these two elements, a new way of accessing the elastic mechanical properties of a material at the micro/nano scale was created. Among the existing models, the once proposed by Oliver and Pharr [8] has been widely applied since it allows to calculate hardness H and the Young's modulus E through a series of equations that relate the main parameters of nanoindentation: the applied load P, the contact depth h_C, and the contact area A_C (h_C). Evaluating the contact area is a quite delicate step since this parameter is directly related to the residual imprint left by the indenter (tip). For this purpose, microscopy observation techniques (AFM or SEM) are required, nevertheless nanoindentation offers the possibility of calculating H and E without the necessity of visualizing the residuals imprints. Indeed, a second alternative statistical method exists to calculate the mechanical properties [8,16–18]. This method is better suited for heterogeneous materials composed by several phases. The main goal of this paper is to isolate the mechanical properties (hardness and Young's modulus) of highly heterogeneous materials (graphite–salt) without having to visualize the residual imprints by a statistical analysis of instrumented indentation technique. Moreover, by using this method we are expecting to obtain key information that could lead us to the selection of the best graphite plus salt candidate (in mechanical terms) to be employed as a PCM material. Previous works related to mechanical characterization of graphite based composite materials can be found in the literature [19–24]. Most of these studies are related to composites made upon graphite and polymers where the mechanical characterization was carried on at the macro scale with standard compression and flexural tests. Moreover, the studied graphites for most of these works, are particle type graphites like flakes, powder or platelets. The mechanical and electrical properties o these different types of graphites can be found on the review performed by Sengupta et al. [19] where a compilation of such variety of graphites was been done. The review also includes graphite based composite materials (graphite and epoxy resins, polymers and alcohols) thus it offers a good vision over the characteristics and applications of graphite and graphite based composites. In terms of mechanical characterization at the micro scale, few works are available. Cho et al. [23] present a multi-scale analysis where graphite–epoxy nanocomposites were characterized by applying analytical and numerical micromechanics models, but no experimental characterization was found. From the point of view of graphite foams like the ones studied in the present work, we can mention the researches of Zhong et al. [20]. Here, a composite material made of graphite foam and an eutectic metal alloy (Bi–Pb–Sn–Cd) was studied. Besides using graphite foams like in our case, the composite's application for this study was also energy storage but again the big difference is that the mechanical characterization was performed at the macro-scale with compression and bending tests. We can see that almost no research can be found about using a micro scale characterization approach for isolating the mechanical properties of specific graphite foam–salt composite materials. The literature shows macro scale mechanical characterizations mostly with particle type graphites composites.

2. Experimental procedure

2.1. Samples preparation

The graphite–salt composites are graphite foams (from Koppers Inc.) infiltrated with sodium nitrate (Scharlab laboratory). Due to the high viscosity of the salt, infiltration of the foam pores cannot be achieved by capillarity. To ensure an optimal infiltration, void has to be created with a pump in order to force the salt through the foam pores. Essentially, the preparation of the samples is as follows: the graphite foam and the salt are placed together inside a stainless steel crucible which is placed inside an oven for several hours (from 6 to 7 h) at 350 °C. Once the salt melted and thus in liquid state, the crucible is extracted from the oven and placed inside a desiccator that has been previously modify by placing at its bottom a mica heater (resistance) working at 370 °C. This mica heater is necessary in order to maintain the salt melted as long as possible while the infiltration takes place. Infiltration begins when the desiccator is closed and the pump turned on. Measurements of the pressure inside the desiccator indicate a pressure of 0.1 bars. After several minutes the pump is stopped and the infiltrated foam is extracted. Knowing the masses before and after the infiltration allows us to calculate the degree of infiltration which indicates a 95% of pore infiltration. Fig. 1 shows the raw materials and the resulting infiltrated foam. Two different types of graphite foams were used to elaborate the graphite–salt composites (Kfoam D1 and L1, in this paper denoted as D and L graphite) in order to see their influence in the mechanical behavior of the samples.

Samples D and L present similar properties in terms of average porosity (70% L; 72% D) and average pore size (600 μm L; 650 μm D). Nevertheless, the big difference between these two samples lies in their density (0.38 g/cm^3 L; 0.48 g/cm^3 D) and coefficient of thermal expansion (3×10^{-6}/°C L; 0.69×10^{-6}/°C D). Moreover sample L presents a

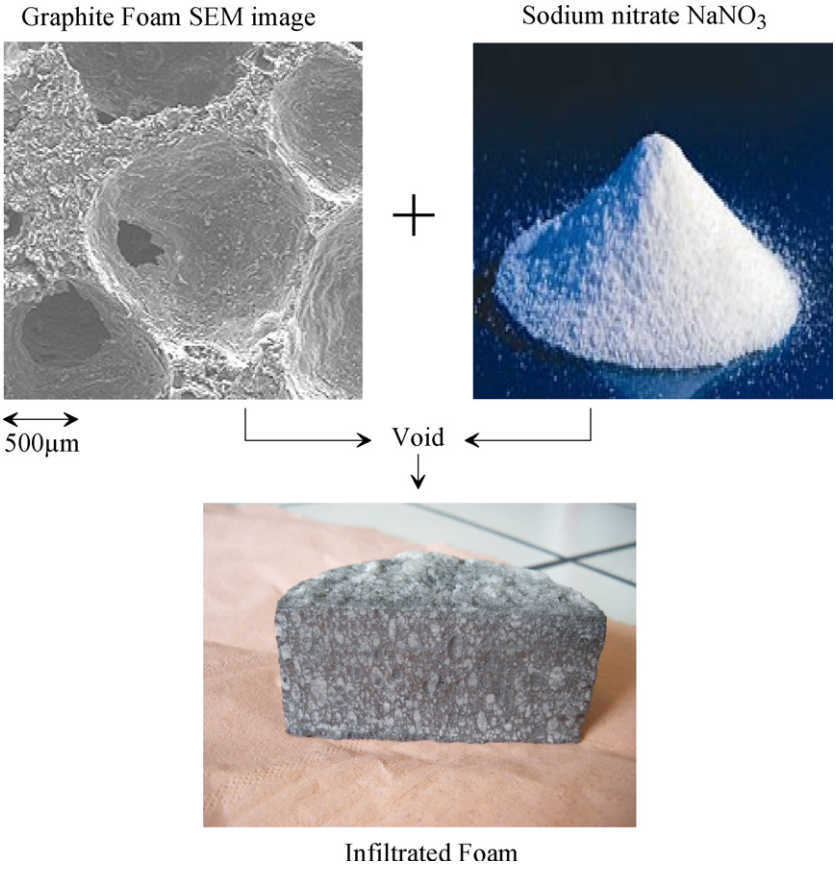

Fig. 1. Schematic representation of the graphite foams salt infiltration.

relative homogeneous structure with pores having similar sizes meanwhile sample D1 has an heterogeneous structure with small and big sized pores. Even if both samples present close average porosity values, their structures are different due to this uneven distribution of pore size present in sample D1. This aspect cannot be seen in the porosity and pore size values since they are average values.

Prior to the nanoindentation tests, the specimens were polished with a dry method, using the following polishing discs: 240, 320, 600, 800, 1200, 2400 and 4000 μm in order to obtain a flat surface. For these kinds of samples, the diamond suspensions and colloidal silica have not been employed in order to reduce the modification of the salt.

2.2. Microstructural characterization

The microstructure of the samples was studied using optical microscopy (OM). We have also performed Scanning Electron microscopy (SEM, Jeol JSM-840) coupled with EDXS (INCA Energy 250, Oxford Instruments) for chemical analysis experiments on graphite–salt composites.

2.3. Nanoindentation tests

Nanoindentation test were performed with a Nano Indenter XP System (Agilent Technologies) with a constant strain rate helded at 0.05 s^{-1} equipped with a Berkovich indenter. The indenter shape has been carefully calibrated for true indentation depths as small as 50 nm by indenting fused silica samples with a well known Young's modulus of 72 GPa [8,12]. The Nanoindentation experiments were performed at constant indentation depth (200 nm) in order to isolate the mechanical properties of each phase (graphite, salt and the interface graphite–salt).

To ensure there was a sufficient population of tests to conduct a statistical study, an array of 32 × 32 indentations with 4 μm spacing were performed at 200 nm of indentation depth. The loading–unloading curve for each tests are recorded, and the H and E are directly obtained from the elastic unloading curve using the Oliver and Pharr approach [8,12,25,26].

3. Statistical method

The sketch presented in Fig. 2 helps to illustrate the advantage of the statistical method for heterogeneous materials. Here the important parameter is the indentation depth h, when tests are performed at important indentation depths, the recorded response of the material will correspond to the average response of all the phases present in the composite. On the contrary when the nanoindentation tests are carried out at small scale, the contribution of each of the phases present in the sample can be isolated and thus their mechanical properties can be obtained due to the size of the residual imprint which is lower than the secondary phase [14,17].

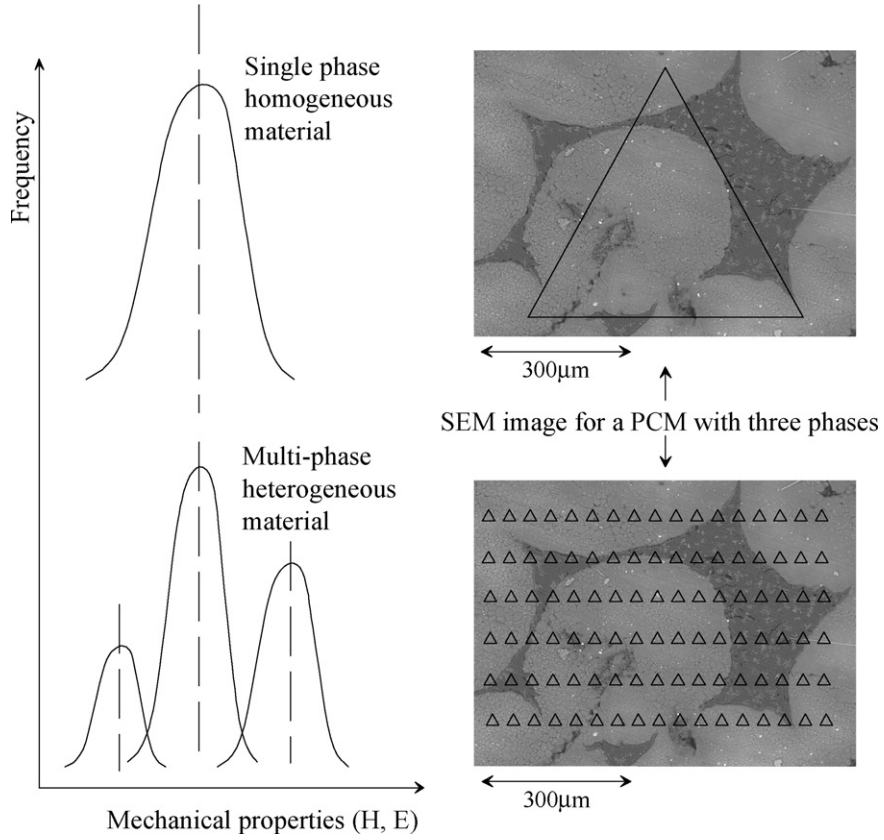

Fig. 2. Statistical method sampling illustration over a graphite–salt PCM sample. Adapted from Constantinides et al. [14,17,18].

Let's first consider an heterogeneous material composed by several phases having each one its own mechanical properties and a characteristic diameter. We can consider two different scenarios; when the residual imprint is lower than the size of the different inclusions, and when the imprint has been performed at higher loads and the residual imprint is higher than the secondary phases. Fig. 2 shows the two possible cases:

(i) The first scenario (upper part of figure) corresponds to a test carried out at important indentation depths, this is represented by a big sized triangle (tip of the indenter) over the SEM image. As previously mentioned, the response of the material will be the same as for a single phase material i.e. a single Gaussian distribution peak.
(ii) The bottom part of scheme is associated with a series of tests carried out at small indentation depths represented here by an array of small triangles over the SEM image, usually named an indentation grid. The response to the applied load in this case is represented by the three Gaussian distribution peaks on the left, each one associated to a phase: salt, graphite and the interface graphite/salt.

Finally it is important to mention that having an important number of indentations will increase the accuracy of the results as expected for any experiment.

As mentioned before, the data coming from the nanoindentation tests can be treated and interpreted by means of a statistical approach. Consider a sample composed by several j phases with sufficient contrast in their mechanical phase properties. Let us assume that the distribution (p_j) of the mechanical properties (x = H and/or E) of each of these j phases is assumed to obey a Gaussian distribution [14,17,18,27]:

$$p_j = \frac{1}{\sqrt{2\pi\sigma_j^2}} \exp\left(-\frac{(x-\mu_j)^2}{2\sigma_j^2}\right) \quad (1)$$

where σ_j is the standard deviation and μ_j the arithmetic mean for each of the number of indentations (N_j) on the material (j) phases. The cumulative distribution function can be written as:

$$\mathrm{CDF} = \sum_j \frac{1}{2} f_j erf\left(\frac{x-x_j}{\sqrt{2}\sigma_j}\right) \quad (2)$$

where x is the mechanical property (H or E plotted in the x-axis), x_j is the mechanical property for each phase and f_j is defined as the relative fraction occupied by each phase and defined as:

$$f_j = \frac{N_j}{N} \quad (3)$$

where N_j parameter corresponds to the number of indentations performed in each phase and N is the total number of imprints performed on the sample of study. This relative fraction must also obey to the following equation:

$$\sum_{j=1}^{n} f_j = 1 \tag{4}$$

Once the experimental CDF is obtained, a deconvolution procedure is applied and the mechanical properties of each of the phases present in the sample can be estimated.

4. Results and discussion

4.1. Microstructure

The two studied samples (D and L) present a density of pores of different size yielding to a different heterogeneous distribution for each sample, as can be observed in Fig. 3. We also see that in both cases (Fig. 3a and b) the salt grains exhibit some cracks that pass through their middle section. This aspect might be related to the solidification process of the salt and the resulting thermo-mechanical stresses displayed between the salt and the graphite matrix. Several factors influence the salt solidification process, like the contrast between the thermal properties of salt and graphite [28–30]. When the sample has just been elaborated and the salt that has been infiltrated inside the pores starts to cool and solidify, the salt grain can be seen as an apparent sphere (in a 2D surface) in contact with an isothermal surface which is the graphite pore wall. This means that the salt grain will start to solidify from the outside to the inside or in other terms the areas closer to the graphite pore walls will be the first to crystallize; and the middle of the grain will be the last. As far as crystallization process goes further, mechanical stresses related to the contrast between the mechanical properties of salt and graphite appear, generating the cracks visible in the SEM images of Fig. 3. Moreover the difference between the thermal expansion coefficient of the graphite and the salt [30,31], creates some residual stresses in the interface generating some cracks at this level during the undercooling process, as observed in Fig. 4. Each grain consists of salt (≅500 μm and 300 μm for D and L samples, respectively) alternating with graphite walls (≅100–200 μm wide). As we can observe in this figure, the graphite employed plays an important role since we can obtain a quasi-homogeneous material, which is likely the case of the samples D, where the crack width at the interface is between 1 and 3 μm. However, in the second case (Fig. 4b), the crack is higher than 5 μm. That means that, the expansion coefficients of each of the employed graphite are significantly different. This hypothesis is in correct agreement with the different values obtained in the literature ($0.69 \times 10^{-6}\,^{\circ}C^{-1}$ and $3 \times 10^{-6}\,^{\circ}C^{-1}$ for D and L samples, respectively [30]).

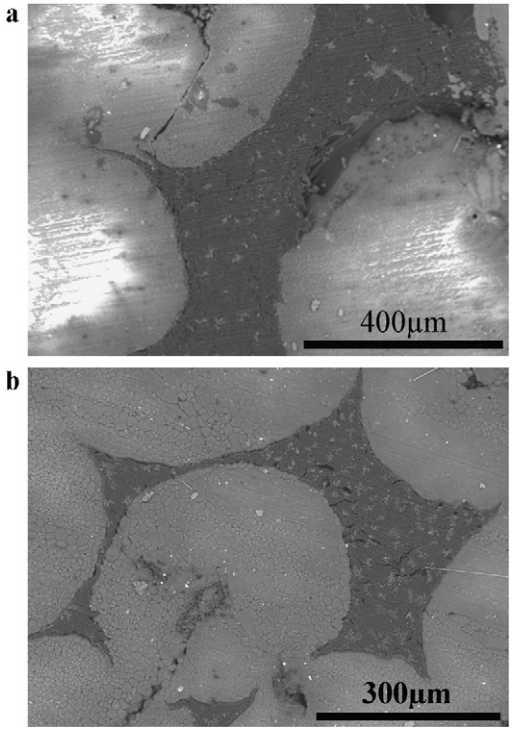

Fig. 3. SEM image for each studied samples. (a) Sample D, and (b) sample L.

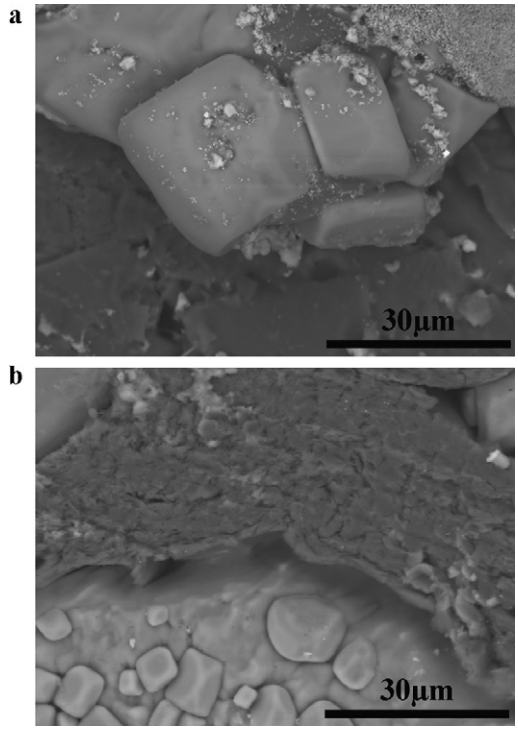

Fig. 4. SEM images of the interphase (graphite/salt) for each studied samples. (a) Sample D, and (b) sample L.

4.2. Statistical method

In order to obtain representative distributions of the mechanical properties in heterogeneous materials, a grid of 1000 indentations was performed in each sample, and then tested like statistical events (see Section 3). Mechanical response distribution represented as frequency plots are

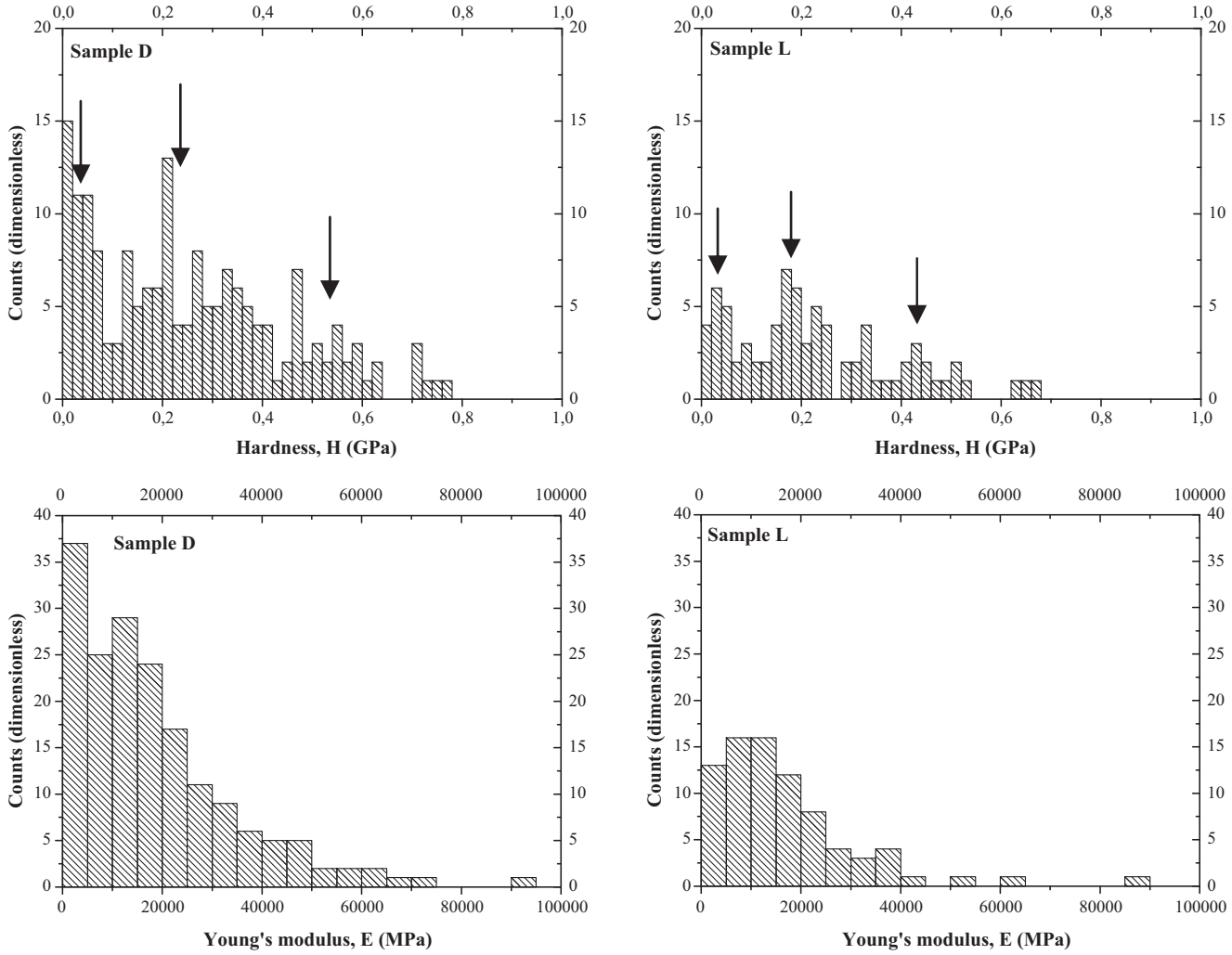

Fig. 5. Frequency plots of the indentation hardness and Young's modulus for the different studied materials. Hardness bin size = 0.02 and Young's modulus bin size = 5000.

employed to analyze indentation data on a composite material. Fig. 5 shows the distribution of the nanoindentation H and E results for the samples D and L.

The different Hardness histograms presented in Fig. 5 exhibit several peaks, thus are related with the hardness value of each phase (see black arrows). However, this effect is not clearly observed in the Young's modulus histogram. As we can see in this figure, some peaks tend to be more distinct for H than E because the volume of material solicited plastically is smaller than that elastically.

In order to observe, discuss and clarify these results without the influence of bin size, the results were represented by cumulative density functions, by assuming that the density functions are correctly fitted by Gaussian distributions. This approach has also been reported in other studies performed on heterogeneous materials [14,17,18,27]. The mean values μ_j^H and μ_j^E, and the standard deviations σ_j^H and σ_j^E, for each mechanical property, H and E distributions, were acquired by fitting the cumulative distribution functions (CDF), using a special sigmoid shape error function, defined in Eqs. (1) and (2). For our heterogeneous materials with three different phases

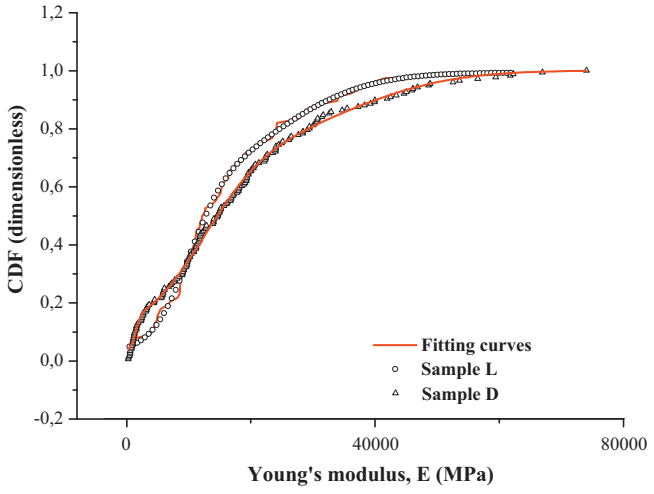

Fig. 6. Statistical indentation analysis of samples D and L. The cumulative distribution function (CDF) of graphite plus Salt samples (samples L and D).

(graphite, salt and the interface) Eq. (3) can be re-written as follow:

$$f(x) = \mathrm{CDF} = \frac{1}{2} f_{\mathrm{graphite}} erf\left(\frac{x - x_{\mathrm{graphite}}}{\sqrt{2}\sigma_{\mathrm{graphite}}}\right) + \frac{1}{2} f_{\mathrm{salt}} erf\left(\frac{x - x_{\mathrm{salt}}}{\sqrt{2}\sigma_{\mathrm{salt}}}\right) + \frac{1}{2} f_{\mathrm{interface}} erf\left(\frac{x - x_{\mathrm{interface}}}{\sqrt{2}\sigma_{\mathrm{interface}}}\right) \quad (5)$$

During the deconvolution process in which Eq. (5) was used to obtain the mechanical response of each phase, several restrictions were programmed: the sum of the total area (f_j) or the surface fraction of each phase was set at 1, and the fitting process was programmed to be completed when the tolerance of the chi-square (χ^2) was less than 1×10^{-15}. Fig. 6 plots the experimental data as well as the fitting for the Young's modulus CDF curves for each sample of study (the hardness CDF curves are not shown but exhibit the same tendency). Table 1 summarises the different parameters obtained by application of the deconvolution technique. The different data and the respective standard errors are listed in the same table. These values show that Eq. (5) fits with high accuracy the different nanoindentation values for each sample. Moreover, the most important result is that we can isolate the mechanical properties for each phase without the need to visualize the different imprints.

Fig. 7 exhibits the plots of H and E distribution for the D sample obtained for each phase using the different parameters

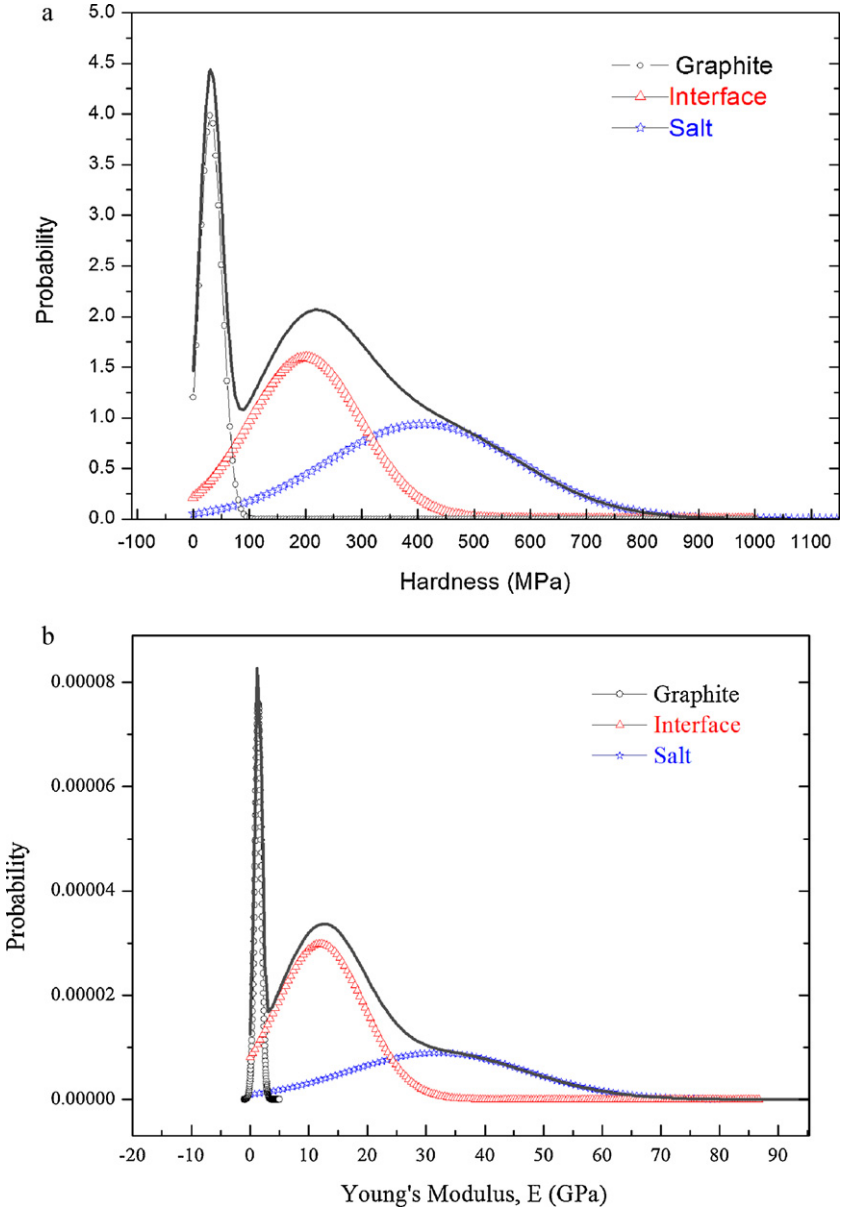

Fig. 7. Distributions simulated using the CDF fitting parameters presented on Table 1 for the D sample. (a) Hardness distribution and (b) Young's modulus distribution.

Table 1
Summary of the different results obtained after the CDF fitting for each sample.

Samples	Phase	MPa		%	Adj. R^2	χ^2	MPa		%	Adj. R^2	χ^2
		μ^H	σ^H	f_j			μ^E	σ^E	f_j		
D	Graphite	31	1	19.3	0.9989	9.67×10^{-5}	1413	59	10.58	0.9985	1.22×10^{-4}
	Salt	489	6	40.6			31,996	518	33.87		
	Interphase	242	9	40.1			12,000	250	55.55		
L	Graphite	35	3	13.5	0.9992	9.85×10^{-5}	1225	42	19.52	0.9965	2.98×10^{-4}
	Salt	426	5	17.6			32,152	425	62.15		
	Interphase	205	2	68.9			15,650	150	18.33		

reported in Table 1 (plots for the L sample are not shown). As we can observe in Table 1, the values greater than $H = 400$ MPa and $E = 30{,}000$ MPa are attributed to indentation on residual salt particles present in the material. This phase present a higher mechanical property due to the fact that the atomic bond of salt particles is stronger than graphite. In the case of salt they present and ionic bond, on the other hand, the graphite presents a covalent bond and also a nanolaminar structure which reduces drastically the mechanical properties of this phase. As we can observe in Table 1, the different interface values are strongly affected depending on the kind of graphite employed. As we discussed previously in the microstructure section, the expansion coefficient for the sample D is lower than the sample L yielding in several microcracks between the graphite and salt. In that case, when the resulting indentation is close to the interface, the elastic field generated during the indentation process, is strongly reduced by this crack which acts dissipating energy. The main concern about this difference in the Young's modulus value in the interface is that it can produce a reduction in the lifetime of these materials since they are going to be used as PCMs and thus they will be continuously subjected to heating/cooling cycles at least one time per day. By using the statistical technique, we can conclude that the best graphite candidate that will supply a longer lifetime is the graphite of the sample D as it has a Young's modulus closer to that of the salt than the sample L.

The different results supplied in Table 1 cannot be compared with a bibliographic results due to this is the first time that the mechanical interaction between each phase in this material is studied.

5. Conclusions

The grid indentation technique has been employed to isolate the mechanical properties of a heterogeneous material. This technique is a powerful tool for examining the properties of constituent phases independently of each other in composite material microstructures without the need to observe the residual imprints. Moreover, we can isolate the mechanical properties (hardness and Young's modulus) for individual phases, as well as their surface volume fractions. This technique and the statistical analysis explained in this paper can also be employed to other composite materials containing mixture of constituent phases distributed randomly.

Statistical indentation analysis allows isolating the hardness, Young's modulus and the superficial partial fraction for each phase of phase change materials at nanometric scale. Moreover, the different result supplied by the deconvolution process allows representing the mechanical properties for each phase as a normal density function.

The results showed a strong dependence on the graphite employed (sample L or D) due to the different residual stresses generated during the solidification process which generate a bad interface (salt–graphite) yielding a considerable reduction in the interface Young's modulus ($E_L = 12{,}000 \pm 250$ MPa and $E_D = 15{,}650 \pm 150$ MPa). The obtained results set the basis for understanding the behavior of graphite foam–salt PCM composite materials for energy storage at the micro scale where interesting phenomena linked to the phase change of the salt appear and influence the graphite foam structure. To complete the mechanical characterization, a macro structure mechanical characterization must be done like micro compression tests. Nevertheless, it is important to mention that selection of the best type of graphite and salt must also rely on a thermal analysis since the main objective of the PCM will be to store and deliver as much energy as possible in an efficient way.

Acknowledgements

The authors thank the Serveis Cientificotécnics of the University of Barcelona (SCT-UB) for the SEM data. The Cost (European Cooperation in Science and Technology) Action TU0802 Program and Conacyt (Consejo Nacional de Ciencia y Tecnologia) from Mexico.

References

[1] A. Sharma, V.V. Tyagi, C.R. Chen, D. Buddhi, Review on thermal energy storage with phase change materials and applications, Renewable and Sustainable Energy Reviews 13 (2009) 318–345.
[2] H. Mehling, L.F. Cabeza, Heat and Cold Storage with PCM: An up to Date Introduction into Basics and Applications, Springer-Verlag, Berlin, Heidelberg, 2008.
[3] F. Kuznik, D. David, K. Johannes, J.J. Roux, A review on phase change materials integrated in building walls, Renewable and Sustainable Energy Reviews 15 (2011) 379–391.
[4] V.V. Tyagi, D. Buddhi, PCM thermal storage in buildings: a state of the art, Renewable and Sustainable Energy Reviews 11 (2007) 1146–1166.
[5] J. Lopez, Z. Acem, E. Palomo del Barrio, $KNO_3/NaNO_3$–graphite materials for thermal energy storage at high temperature: Part I. Elaboration

methods and thermal properties, Applied Thermal Engineering 30 (2010) 1580–1585.
[6] M.M. Kenisarin, High-temperature phase change materials for thermal energy storage, Renewable and Sustainable Energy Reviews 14 (2010) 955–970.
[7] A. Gil, M. Medrano, I. Martorell, A. Lázaro, P. Dolado, B. Zalba, L.F. Cabeza, State of the art on high temperature thermal energy storage for power generation. Part 1. Concepts, materials and modellization, Renewable and Sustainable Energy Reviews 14 (2010) 31–55.
[8] W.C. Oliver, G.M. Pharr, Measurement of hardness and elastic modulus by instrumented indentation: Advances in understanding and refinements to methodology, Journal of Materials Research 19 (2004) 3–20.
[9] Y.T. Cheng, C.M. Cheng, Scaling, dimensional analysis, and indentation measurements, Materials Science & Engineering R-Reports 44 (2004) 91–149.
[10] J.J. Roa, E. Jiménez-Piqué, T. Puig, X. Obradors, M. Segarra, Nanoindentation of multilatered epitacial $YBa_2Cu_3O_{7-\delta}$ thin films and coated conductors, Thin Solid Films 519 (2011) 2470–2476.
[11] J.J. Roa, E. Gilioli, F. Bissoli, F. Pattini, S. Rampino, X.G. Capdevila, M. Segarra, Study of the mechanical properties of CeO_2 layers with the nanoindentation technique, Thin Solid films 518 (2009) 227–232.
[12] W.C. Oliver, G.M. Pharr, An improve technique for determining hardness and elastic modulus using load and displacement sensing indentation experiments, Journal of Materials Research 7 (1992) 1564–1583.
[13] F.-J. Ulm, M. Vandamme, C. Bobko, J.A. Ortega, K. Tai, C. Ortiz, Statistical indentation techniques for hydrated nanocomposites: concrete, bone and shale, Journal of the American Ceramic Society 90 (2007) 2677–2692.
[14] G. Constantinides, F.-J. Ulm, K. Van Vliet, On the use of nanoindentation for cementitious materials, Materials and Structures 36 (2003) 191–196.
[15] G. Sundararajan, M. Roy, Hardness testing, encyclopedia of materials, Science and Technology 1 (2001) 3728–3736.
[16] N.X. Randall, M. Vandamme, F.-J. Ulm, Nanoindentation analysis as a two-dimensional tool for mapping mechanical properties of complex surfaces, Journal of Materials Research 24 (2009) 679–690.
[17] G. Constantinides, F.-J. Ulm, The nanogranular nature of C–S–H, Journal of the Mechanics and Physics of Solids 55 (2006) 64–90.
[18] G. Constantinides, K.S. Ravi Chandran, F.-J. Ulm, K.J. Van Vliet, Grid indentation analysis of composite microstructure and mechanics: principles and validation, Materials Science and Engineering A 430 (2006) 189–202.
[19] R. Sengupta, M. Bhattacharya, S. Bandyopadhyay, A.K. Bhowmick, A review on the mechanical and electrical properties of graphite and modified graphite reinforced polymer composites, Progress in Polymer Science 36 (2011) 638–670.
[20] Y. Zhong, Q. Guo, S. Li, J. Shi, L. Liu, Thermal and mechanical properties of graphite foam/Wood's alloy composite for thermal energy storage, Carbon 48 (2010) 1689–1692.
[21] A. Alrashdan, A. Turki Mayyas, S. Al-Hallaj, Thermo-mechanical behaviours of the expanded graphite-phase change material matrix used for thermal management of Li-ion battery packs, Journal of Materials Processing Technology 210 (2010) 174–179.
[22] K. Kalaitzidou, H. Fukushima, L.T. Drzal, Mechanical properties and morphological characterization of exfoliated graphite–polypropylene nanocomposites, Composites Part A, Applied Science and Manufacturing 38 (2007) 1675–1682.
[23] J. Cho, J.J. Luo, I.M. Daniel, Mechanical characterization of graphite/epoxy nanocomposites by multi-scale analysis, Composites Science and Technology 67 (2007) 2399–2407.
[24] N. Cunningham, M. Lefèvre, J.P. Dodelet, Y. Thomas, S. Pelletier, Structural and mechanical characterization of as-compacted powder mixtures of graphite and phenolic resin, Carbon 43 (2005) 3054–3066.
[25] J.J. Roa, X.G. Capdevila, M. Martínez, F. Espiell, M. Segarra, Nanohardness and Young's modulus of YBCO samples textured by the Bridgman technique, Nanotechnology 18 (2007) 385701/1–385701/6.
[26] J.J. Roa, A. Magrasó, M. Morales, P. Núñez, M. Segarra, Determination of hardness, Young's modulus and fracture toughness of lanthanum tungstates as novel proton conductors, Ceramics International 37 (2011) 1593–1599.
[27] E. Rayon, V. Bonache, M.D. Salvador, J.J. Roa, E. Sanchez, Hardness and Young's modulus distributions in atmospheric plasma sprayed WC–Co coatings using nanoindentation, Surface & Coatings Technology 205 (2011) 4192–4197.
[28] Y. Nagasaka, A. Nagashima, The thermal conductivity of molten $NaNO_3$ and KNO_3, International Journal of Thermophysics 12 (1991) 769–781.
[29] H. Bloom, A. Doroszkowski, S.B. Tricklebank, Molten salt mixtures. IX. The thermal conductivities of molten nitrate systems, Australian Journal of Chemistry 18 (1965) 1171–1176.
[30] http://www.kfoam.com/mainsite/material (accessed 17.06.2011).
[31] M.Md. Ibrahim, V. Ramachandran, K. Sarangapani, R. Srinivasan, Thermal expansion of sodium nitrate (I), Journal of Physics and Chemistry of Solids 47 (1986) 517–520.